Title

KOH activated carbon/graphene nanosheets composites as high performance electrode materials in supercapacitors

Journal

RSC Advances, 4(90)

ISSN

2046-2069

Authors

Yu, Shengming
Li, Yueming
Pan, Ning

Publication Date

2014

DOI

10.1039/c4ra06710j

Peer reviewed

Journal Name

RSCPublishing

ARTICLE

Cite this: DOI: 10.1039/x0xx00000x

Received 00th January 2012,
Accepted 00th January 2012

DOI: 10.1039/x0xx00000x

www.rsc.org/

KOH activated carbon/graphene nanosheets composites as high performance electrode materials in supercapacitor

Shengming Yu,[a] Yueming Li[a*] and Ning Pan[b*]

The importance of developing high performance electrode materials with low cost for supercapacitor is self-evident. In this paper, KOH activated carbon/graphene nanosheet composites were prepared via a simple hydrothermal treatment of graphite oxide and KOH activated carbon. Next electrochemical experiments conducted have demonstrated that these composites exhibited synergistically improved electrochemical performance as electrodes in supercapacitor. The specific capacitance of these composites can reach as large as 205 and 173 F g^{-1} in 6M KOH aqueous solution and 1M $TEABF_4$ in acetonitrile solution respectively. In addition, as fabricated electrodes using these composites show a reduced internal resistance and higher capacitance retention performance. Furthermore, the entire preparation process is simple, low cost and easily scalable to mass production, leading to great potential for composites.

1 Introduction

Supercapacitors have drawn much attention due to their high power density, long cycle life, low maintenance and fast dynamics of charge process.[1-3] There are mainly two mechanisms for supercapacitor to store energy. One establishes capacitance via electrical double layer through the separation of opposite charges at the interface between electrode and electrolyte. The other is pseudocapacitance mechanism with reversible Faradiac redox reaction.[4] Needless to say, the electrode materials used in supercapacitor play critical role in determining the electrochemical performance of supercapacitor. Up to now, the electrode material used in most commercialized supercapacitor is activated carbon due to its low cost, large specific surface area (SSA) and good chemical stability. However, the specific capacitance of activated carbon is low due to presence of lots of non-accessible pore by electrolyte. Furthermore, the conductivity of activated carbon is poor due to the defective nature.[5] To circumvent such disadvantages of activated carbon, novel carbon materials such as carbon nanotube, mesoporous carbon and graphene nanosheets have been studied. [2]

Among these novel materials, graphene nanosheets have shown promising potentials as electrode material in supercapacitor. Graphene, a two dimensional (2D) material,[6] has remarkable properties in respect of optics, mechanics, magnetics, and electrics.[7-9] It has a specific surface area (SSA) as much as 2630m^2 g^{-1} and can provide a specific capacitance up to 550 F g^{-1} in theory. Furthermore, the electrical conductivity and chemical stability of graphene are superior, very important parameters for electrode materials in supercapacitor. [6,10,11] Recent years, a plenty of researches have been carried out to study graphene-based supercapacitor, and some substantial progresses have been made.[12-24] However, some issues still remain to be overcome. For example, graphene tends to agglomerate and restack into graphite due to van der Waals attraction and strong π-π interaction, thus greatly lowering the SSA, actual specific capacitance and conductivity.[25-27] Also, the preparation of graphene is complicated, resulting high production cost and as the result limiting the application of graphene on a large scale.

Considering the low cost of activated carbon and better performance of graphene nanosheets, activated carbon (AC)/graphene nanosheets composites become a logical choice to achieve some synergy by mixing the two materials. For example, Li *et al*. prepared graphene/AC composites via hydrazine reduction of graphite oxide and acid treated commercial AC, which showed a specific capacitance of 181 F g^{-1} at a scan rate of 1 mV s^{-1} in 1 M NaCl solution. [28] Chen et al prepared graphene/AC composites by KOH activation of oligomers of p-phenylene diamine and graphite oxide, which showed a specific capacitance of 122 F g^{-1} at 0.1 A g^{-1} in KOH electrolyte.[29] And Zhou et al prepared through solvothermal treatment of graphite oxide and acid treated AC, which also showed good electrochemical performance in an organic electrolyte.[30]

Although the graphene/AC composites have shown potential as electrode materials, their performance is not satisfying especially in rate performance.[28-30] KOH activation has shown to be an effective way to modify the properties of activated carbon, thus greatly boosting the electrochemical performance.[31-34] Herein, we report on preparation a composite

of graphene, via hydrothermal treatment of GO and KOH activated carbon. The as prepared graphene/KOH activated carbon not only showed a high specific capacitance but also showed excellent rate performance.

2 Experimental

2.1 Synthesis of graphene oxide (GO)

Graphene oxide was prepared from nature graphite powder (325 mesh) according to the modified Hummers' method.[35,36]

2.2 Treatment of activated carbon with KOH

Commercial AC was mixed with KOH at the mass ratio of AC: KOH=1:4, grinded sufficiently and then heated at 800 °C under an N_2 atmosphere for 1h. The mixture was immersed in 0.1 M HCl aqueous solution and then washed and filtered with de-ionized water until the filtrate become completely neutral. Finally, the product was dried at 80 °C for 24h, and denoted as KAC.

2.3 Synthesis of Graphene/KAC composites

Briefly, 60 mL of 1mg/mL GO solution was mixed with 60, 120, 180 mg KAC respectively, then sonicated and stirred to form a uniform dispersion. The dispersions were transferred to a sealed Teflon-lined autoclave and heated 180 °C for 12 h. The products were filtered, washed with de-ionized water and freeze dried in vacuum. We denoted the products as GKAC1(GO:KAC,1:1 mass ratio), GKAC2 (GO:KAC,1:2) and GKAC3 (GO:KAC, 1:3), corresponding to the increasing amount of KAC used. For comparison, graphene nanosheets were also prepared with the same reaction condition except that no KAC was added, and the sample was denoted as RGO.

2.4 Characterization

Scanning electron microscope (SEM) images were recorded using a Hitachi S 4800 scanning electron microscope. The X-ray diffraction (XRD) measurements of the samples were carried out in a Rigaku D/ max 2500 X-ray powder diffractometer using a graphite monochromator with Cu Kα radiation (λ=1.5406 Å). The data were collected between scattering angles (2θ) of 5-80° at a scanning rate of 4°/min. Fourier transform infrared spectroscopy (FT-IR) were conducted on Bruker E55 FT-IR spectrometer in the range of 4000-400 cm^{-1}. N_2 adsorption/desorption isotherms were obtained by a gas adsorption analyzer (ASAP 2020, Micromeritics Instrument Co. USA) at 77K.

2.5 Electrochemical measurement

To evaluate electrochemical performance in aqueous solution, an electrode material was prepared using the graphene/KAC composites, mixed with the conductive carbon black and Polytetrafluoroethylene (60% emulation, Aldrich), in the weight ratio 85:10:5. The mixture was prepared as slurry in ethanol and spread onto nickel foam with spatula. The pasted nickel electrodes were dried at 120 °C under vacuum for 12h and then pressed at a pressure of 5 MPa for 1 min. Two-electrode system was used for all the electrochemical tests. The symmetric supercapacitor was assembled in a Swagelok cell, with microporous polypropylene as separator between the electrodes. The electrolyte used was 6 M KOH aqueous solution. Assembled cells were allowed to soak electrolyte overnight.

The electrode used in organic system is fabricated as follows. The electrode materials were prepared using as prepared samples, mixed with the conductive carbon black and polyvinylidene fluoride (Aldrich), in the weight ratio 85:10:5. The mixture was prepared as slurry in N-methyl pyrrolidinone and spread onto aluminum foil using the doctor blade technique. The pasted electrodes were then dried at 120 °C under vacuum for 12 h. The symmetric supercapacitor was assembled in a Swagelok cell in argon filled glove box (Braun, H_2O<1 ppm, O_2< 1ppm) with microporous polypropylene as separator between the electrodes. The electrolyte used was 1M tetraethylammonium tetrafluoroborate ($TEABF_4$) in acetonitrile (AN) solution.

The cyclic voltammetry (CV) measurements and electrochemical impedance spectroscopy (EIS) were carried out on an electrochemical workstation (P4000, Princeton Applied Research, USA). The galvanostatic charge/discharge of the assembled cells was performed on Arbin battery testing unit (Arbin Inc., USA). All the measurements were carried out at room temperature. Ragone plots were calculated by using the equations $E=CV^2/(8\times3.6)$ and $P = E/\Delta t$, respectively. (C refers the specific capacitance based on single electrode, Δt is the discharging time).

3 Results and discussions

As shown in Fig. 1, KOH activated AC showed a broad peak at about 22.5°, indicating the amorphous nature. The XRD pattern of GO showed a main peak at about 9.6° (corresponding to interlayer spacing of 0.85 nm), representing the successful oxidation of graphite into graphite oxide. After hydrothermal treatment, the peak at about 9.6 ° disappeared, and the weak and broad peak appeared at about 24.4 ° (002), indicating the reduction of graphite oxide as well as absence of long-range ordering structure. [24] As for GKAC, the XRD results of them are similar to that of KAC on the whole, showing a broad peak at about 23°, consistent with amorphous carbon structure.

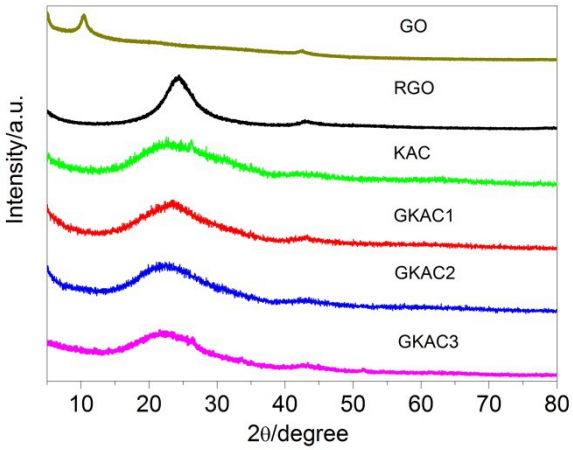

Fig. 1 XRD patterns of GO, RGO, KAC, GKAC1, GKAC2 and GKAC3

As seen in Fig. 2, FT-IR spectrum of GO showed a strong peak at 3600-3300 cm^{-1} attributable to the hydroxyl stretching vibrations of the C-OH groups. The peak at 1420 cm^{-1} is assigned to the O-H deformation, and a weak band at 1734 cm^{-1} is assigned to C=O stretching. The band at about

1620 cm^{-1} is assigned to C-C (sp2) stretching vibration. Peaks at 1220 and 1050 cm^{-1} are assigned to C-O stretching, and 848 cm-1 (weak) to (O-C=O). These values are close to those in previous reports. [37-39] For KAC sample, only one main adsorption band was clearly visible, centered at 1580 cm^{-1} assigned to C=C stretching vibration. After reduction via hydrothermal process, most oxygen-containing groups in the composites have been removed judging from the curves. The emerging peaks at 1580 cm^{-1} can be assigned C=C stretching vibration of aromatic ring and the peak at 1234 cm^{-1} is attributed to C-OH stretching. These data further proved the GO has been reduced into graphene nanosheets through hydrothermal treatment.

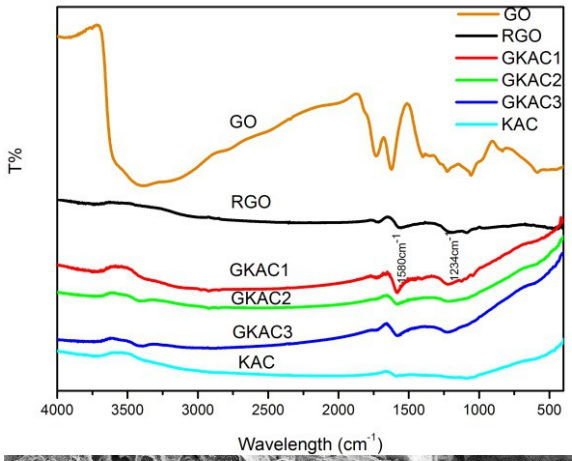

Fig. 2 FT-IR spectra of GO, rGO, GKAC1, GKAC2, GKAC3 and KAC.

Scanning Electron Microscopy (SEM) was used to study the microstructure and morphology of products. As shown in Fig 3(A, B), RGO formed in hydrothermal process by partial overlapping or coalescing of graphene nanosheets, forming an interconnected porous network. The pore sizes of the network are in the scale of submicrometer to several micrometers, and the pore walls possess only few thin layers of stacked graphene sheets, similar to previous reports.[26, 40, 41] The KOH activated AC shows irregular particle morphology, with surface composited of spherical particles of diameter about 100nm, shown in Fig. 3(C). Fig. 3(D-F) shows the SEM images of GKAC2. It can be clearly seen that the surfaces of pure KAC are obviously different to that of KAC in the composites, whose surfaces have been covered with graphene nanosheets after hydrothermal process. It is hence demonstrated that hydrothermal treatment is an efficient and also environmentally friendly route to transform the graphite oxide in to graphene nanosheets, as no toxic reagents such as hydrazine were needed. For our case, the effective coating of graphene layer via hydrothermal treatment helps improve the conductivity of activated carbon. In our case, the effective coating of graphene And the morphologies of both GKAC1 and GKAC3 are similar to that of GKAC2.

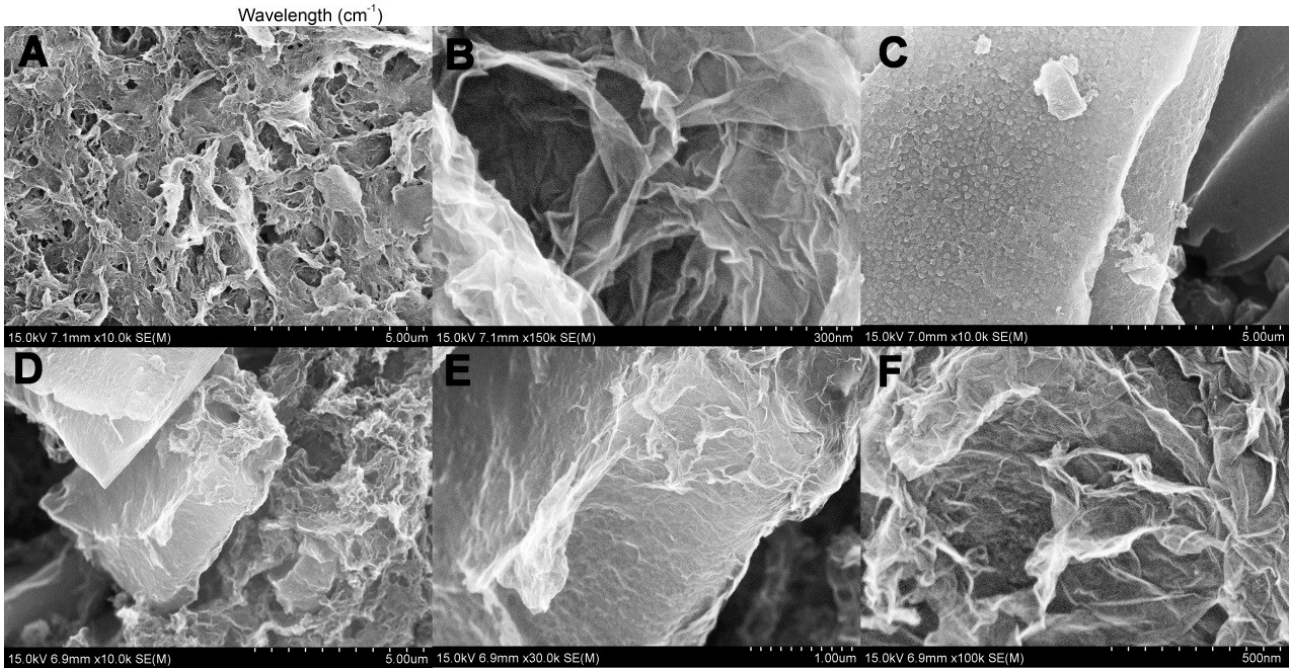

Fig. 3 SEM images of RGO (A, B), KOH activated AC (C), GKAC2 at different magnification (D, E, F).

The nitrogen adsorption/desorption isotherms of various samples are shown in Fig. 4. According to the IUPAC classification, the nitrogen adsorption isotherms of KAC, GKAC2 and pristine AC exhibit both type I characteristics of microporosity and type IV characteristics of mesoporosity, while RGO exhibit mainly characteristic of type IV. The total specific surface area (SSA) of pristine AC evaluated using the Brunauer-Emmett-Teller (BET) equation was 1503 m^2g^{-1}, while that of KAC increased to 3336 m^2g^{-1}. Furthermore, both the micro-pore areas and volume of KAC increased significantly according to Table 1. These experiments indicate that the KOH activation is very effective in increasing the SSA of carbon materials. The SSA of RGO is only about 325 m^2g^{-1}, which is far below the theoretical value (2630 $m^2 \cdot g^{-1}$) of single layer graphene due to aggregation and restack of graphene layers. Although the SSA of RGO is rather low, the GKAC2 still exhibits a SSA of 2806 m^2g^{-1}. Non-local density functional theory (NL-DFT) calculations were believed as the most accurate method to evaluate the pore size distribution of

materials containing micropores structure. [42] As shown in Fig. S1, the pore size calculated by NL-DFT method assuming a slit geometry indicates broad size distribution for RGO, while very narrow size distributions for AC, KAC and GKAC2 (Most pores are micro- and mesopores with sizes of less than 10 nm).

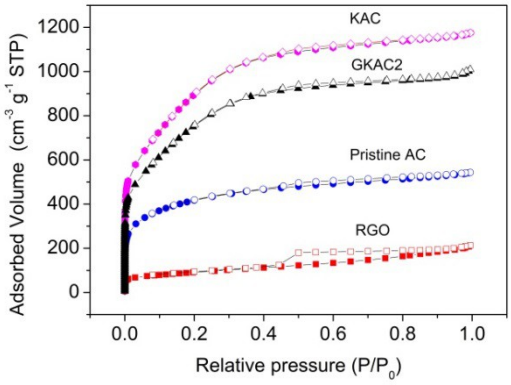

Fig. 4 N_2 Adsorption–desorption isotherms of RGO, pristine AC, GKAC2 and KA**C**

To study the electrochemical performance of as prepared GKAC, cyclic voltammetry (CV) was carried out in an electrochemical window from 0 to 1V in 6M KOH aqueous solution and 0 to 2.3 V in 1M $TEABF_4$ in AN solution at room temperature, respectively. As shown in Fig. 5, nearly rectangular curves can be seen for RGO, GKAC2 and KAC electrodes at low scan rate from 1 to 200 mV·s^{-1}, indicative of a typical electric double layer behavior and good rate performance. It is noteworthy that the integral area for the GKAC2 electrode is largest among three electrodes, indicating the improved electrochemical performance due to the synergetic effects of KAC mixed with graphene nanosheets. The reason we use KOH activated carbon instead of pristine AC is that KAC has a much improved electrochemical performance than pristine AC. This is confirmed in Fig. S2, where the KAC electrode has a larger integral area and more rectangular shape in CV curve than that of pristine AC, indicating improved capacitance as well as decreased resistance. This is further proved by EIS data in Fig. S3. The CV curves for GKAC2, RGO and KAC electrodes in organic electrolyte (1M $TEABF_4$ in AN solution) are also nearly rectangular in shape from 0 to 2.3 V over a wide range of scan rates, indicating an excellent capacitive behavior, shown in Fig. S4.

Galvanostatic charge discharge test was also carried out to further study the electrochemical performance. Consistent to result of CV test, the pristine AC without treatment by KOH, shows a poor electrochemical performance, with a specific capacitance of mere 78 Fg^{-1} at current density of 2 Ag^{-1}, much smaller than that of KAC, shown in Fig. S5. The improved electrochemical performance should be related to the increased SSA due to the KOH activation, as disclosed in Table 1.

Table 1 Porosity properties of the pristine AC, KAC, RGO and GKAC

sample	Total SSA [m^2g^{-1}]^a	Micropore area [m^2g^{-1}]^b	External area [m^2g^{-1}]^b	Micropore volume [$cm^{-3}g^{-1}$]^b	Total volume [$cm^{-3}g^{-1}$]^b	Pore size [nm]^c
Pristine AC	1503	1362	141	0.652	0.841	2.24
KAC	3337	3097	240	1.527	1.818	2.18
RGO	325	156	169	0.081	0.330	4.06
GKAC2	2807	2623	184	1.306	1.562	2.23

a) SSA calculated based on BET method; b) based on t-plot method; c) Adsorption average pore width (4V/A by BET)

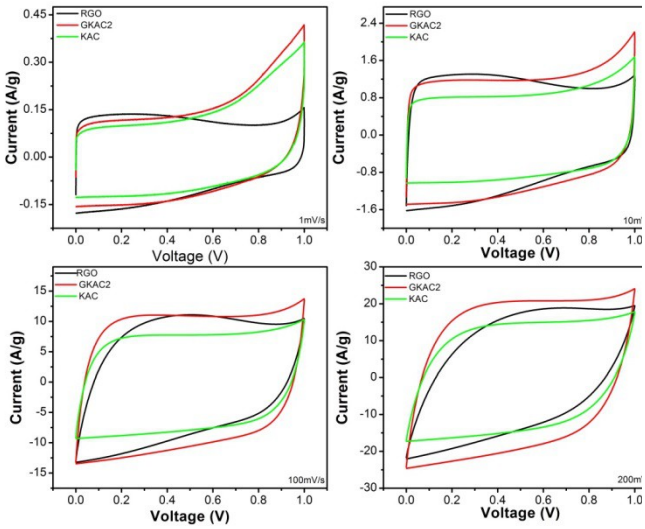

Fig. 5 Cyclic voltammetry curves of RGO, GaAC2, and KAC at various scan rates ranging from 1 to 200mV s^{-1} in 6M KOH aqueous solution

As presented in Fig. 6, the symmetric charge/discharge curves and the linear potential-time profile in the whole potential range for KAC, GKAC2 and RGO demonstrate a capacitive behavior with a rapid I-V response in both aqueous and organic electrolyte. It can be calculated that the KAC and RGO electrodes can deliver a specific capacitance of 126 and 186 F g^{-1} at current density of 2 Ag^{-1} in 6M KOH electrolyte, respectively. It is anticipated that the specific capacitance of composites of KAC and graphene nanosheets should be between the value of pure KAC and that of graphene nanosheets. Although the SSA of AC or KAC is very large, their specific capacitance is still low due to the existence of lots of non-accessible pore by electrolyte. As shown Table 2, GKAC3 electrode indeed delivered a specific capacitance of 164 Fg^{-1}. However, GKAC2 electrode showed a specific capacitance of 205 F g^{-1} at 2 Ag^{-1}, much higher than anticipated values (126 ~ 186 Fg^{-1}), indicating a synergetic effect between graphene nanosheets and KAC. Even in organic electrolyte, GKAC2 can also deliver a specific capacitance of 171 Fg^{-1} at the same current density. The improvement can be attributed to the more accessible surface area for ions due to existence of surface functionality of the composites, improved electrical conductivity owing to the flat graphene structure, and higher electrochemical activity of the synergistically fused hybrid

multidimensional architecture, in which the ions can access the edge or basal planes of graphene and the interior of porous activated carbon easier in composites. [43] Furthermore, as shown in Fig. S1, the composites have more micropores than RGO and more mesopores than activated carbon, the suitable pore distribution also contribute to the better electrochemical properties for composites.

Table 2 Specific capacitance at current density of $2Ag^{-1}$ for as prepared samples

Current Density	KAC (Fg^{-1})	GKAC1 (Fg^{-1})	GKAC2 (Fg^{-1})	GKAC3 (Fg^{-1})	RGO (Fg^{-1})
2(Ag^{-1})	126	188	205	164	186

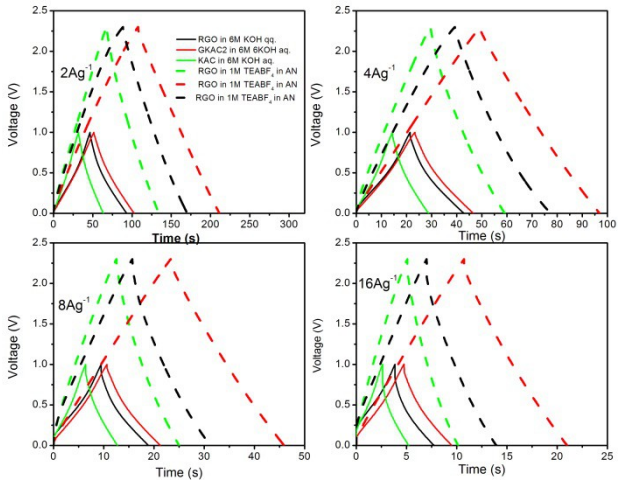

Fig. 6 Galvanostatic charge/discharge curve of RGO, GKAC2, and KAC at the current density of 2, 4, 8 and 16A g^{-1} in 6M KOH aqueous solution and 1M $TEABF_4$ in AN solution

To further study the rate performance for as prepared products, higher current density ranging from 4 to 16A g^{-1} were carried out for RGO, GKAC2 and KAC electrodes. Even in higher rate, GKAC2 electrode demonstrated higher specific capacitance as well as low internal resistance (IR) drop, indicating superior electrochemical performance as electrode materials for supercapacitor. The GKAC2 electrode shows the smallest IR drop among these electrodes, likely due to the coating of graphene on the surface of KAC. The low internal resistance here can be attributed to a couple factors. First, the graphene nanosheets strongly bonded on the surface of KAC helped to improve the conductivity of KAC because the flat graphene nanosheets on the surface of KAC will not aggregate seriously due to the solid support of KAC. On the other hand, the conductive networks formed between the graphene and KAC facilitated the ion transportation. [30] Even in higher rate, GKAC2 electrode can also deliver a specific capacitance of 143 Fg^{-1} in organic electrolyte, higher than those of RGO and KAC electrodes in same current density, showing superior rate performance for composites.

Fig. 7 shows the specific capacitance of at varied current density for RGO, GaAC2 and KAC electrodes in aqueous electrolyte. It can be clearly seen that even at current density of $16Ag^{-1}$, the GKAC2 electrode can still deliver a specific capacitance of 152 Fg^{-1} (corresponding to a maximum energy density of 5.3 Wh/kg, according to $E=CV^2/(8\times3.6)$), much higher than that of single KAC (83 Fg^{-1}, corresponding to 2.9 Wh/kg) or RGO (122 Fg^{-1}, corresponding to 4.3Wh/kg) electrodes. Although the specific capacitance (173 Fg^{-1}) at the same current density in organic electrolyte for GKAC2 electrode is slightly lower than that in aqueous electrolyte, the energy density (26.3 Wh/kg) of corresponding supercapacitor is much higher than that (5.3 Wh/kg) of corresponding one in aqueous solution, indicating the excellent performance of GKAC2 as electrode materials.

Note that the overall performance metrics achieved here are much better than the previous values with similar approach (122 Fg^{-1} at 0.1 Ag^{-1} in KOH electrolyte by Chen et al [29], and 117 Fg^{-1} at $1Ag^{-1}$ in organic electrolyte by Zhou et al [30]). Although there are higher values reported by some studies for activated carbon/graphene composites [44, 45], the preparation of AC reported is complicated, time consuming and hard to use on a large scale compared to the use of commercial AC in this study. In addition, the GKAC2 electrode also showed very good capacitance retention performance (over 90 % within 500 cycles at every varied rate), shown in Figure 7(B). And the good cycle performance of GKAC2 electrode has been further confirmed by the high retention rate (about 90% after first 2500 cycles, about 97% for the following 1000 cycle and 98% for another 1000 cycle at current density of 4, 8 and $16Ag^{-1}$, respectively), shown in Fig. S6.

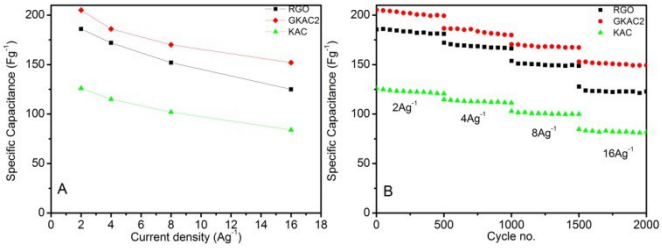

Fig. 7 The specific capacity of RGO, GKAC2 and KAC at the current density of 2, 4 , 8, 16A g^{-1} (A); Cycle stability of RGO, GKAC2 and KAC electrode at varied current density in 6M KOH aqueous solution (B).

The Ragone plots clearly show that both the energy density and power density of supercapacitor in organic electrolyte are much higher than those in aqueous one, shown in Fig. 8A. The energy density of the supercapacitor fabricated with GKAC2 can reach up to 32.2 Wh/kg at the power density of 1.1 kW/kg in organic system, which is much higher than those of KAC and RGO (25.8 and 21.7 Wh/kg, respectively). Even at the power density of 9.1 kW/kg, the GKAC2 supercapacitor can deliver an energy density of 26.3 Wh/kg, clearly exhibiting the superior electrochemical performance of the composites.

Electrical impedance spectroscopy (EIS) was carried out to further examine the electrochemical performances of these materials. The Nyquist plot was performed by conducting ac impedance measurements at a frequency range of 100 kHz to 0.01 Hz. Fig. 8B shows the Nyquist plots of RGO, GKAC2, and KAC electrodesin 6M KOH aqueous solution. At low frequency region, nearly vertical lines can be clearly seen for these three electrodes, indicating ideal capacitive behavior for these electrodes. At the high frequency region, it is observed that semi-circle loop of GKAC2 (shown in Fig. S7) is the smallest among the three electrodes (GKAC2<KAC<RGO), indicating a minimized charge transfer resistance in the GKAC2 electrode. The total equivalent series resistance (ESR) obtained by extrapolating the vertical portion of the plot to the real axis was estimated to be 0.49, 0.6 and 0.85 ohms for

the GKAC2, KAC2, and RGO electrodes, respectively. The small ESR of GKAC2 was consistent with the small IR drop in charge-discharge tests.

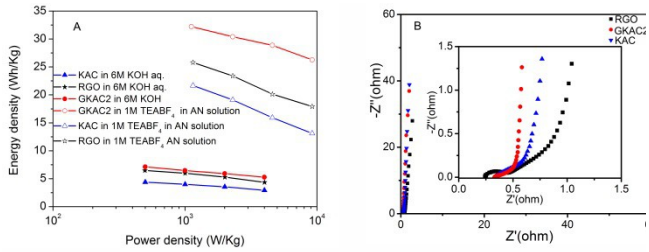

Fig. 8 (A) Ragone plots of RGO, GKAC2, and KAC fabricated supercapacitors; (B) Nyquist plots of RGO, GKAC2 and KAC electrodes in 6M KOH aqueous solution (Inset magnifies the data in the high frequency range)

Based on hydrothermal experiment, the conversion rate of graphite oxide to graphene nanosheets is about 50%. The graphene content in GKAC2 is only about 20%, thus the cost of GKAC2 is rather low compared with pure graphene nanosheets. Furthermore, the electrochemical performance of GKAC2 is much better than those of pure graphene nanosheets or pure KOH activated carbon. Therefore, the composites of graphene/KOH activated are very promising in potential application in supercapacitor.

4. Conclusions

Using a composite by mixing the graphene (RGO) and KOH activated carbon (KAC) at an optimized blend ratio of 1:2 (RGO:KAC), we prepared electrodes for supercapacitors. The new electrodes exhibited a significant synergy, including a much improved specific capacitance in both aqueous and organic solution electrolyte, a high energy density (26.3 Wh/Kg) even at high current density (16 Ag^{-1}) in organic system, a reduced internal resistance and excellent capacitance retention, than those of either pure KAC or pure RGO counterparts.

The entire process is simple, environmentally benign and easily scalable to mass production. Considering the high price of pure graphene or RGO, mixing KAC into the structure also significantly reduce the cost.

Acknowledgements

The authors acknowledge the financial support from National Natural Science Foundation of China (Grant No. 51202212) and Natural Science Foundation of Hebei Province (Project No. E2014203033).

Notes and references

[a] State Key Laboratory of Metastable Materials Science and Technology, College of Materials Science and Engineering, Yanshan University, Qinhuangdao, Hebei Province, 066004, China.

[b] Nanomaterials in the Environment, Agriculture, and Technology (NEAT)

University of California at Davis, CA, 95616.

* Corresponding author: Dr. Yueming Li, E-mail: liyueming@ysu.edu.cn and Prof. Ning Pan, E-mail:npan@ucdavis.edu.

Electronic Supplementary Information (ESI) available: [**Fig. S1**, Pore size distribution curves; **Fig. S2**, CV curves of pristine AC and KAC; **Fig. S3**, Nyquist plots of pristine AC and KAC electrodes, **Fig. S4** Cyclic voltammetry curves of RGO, GaAC2, and KAC electrodes at various scan rates in 1M $TEABF_4$ in AN solution; **Fig. S5**, Charge-discharge curves of pristine AC and KAC electrodes and **Fig. S6** Nyquist plots of pristine GKAC2 electrodes at high frequency]. See DOI: 10.1039/b000000x/

1. P. Simon and Y. Gogotsi, *Nat. materials*, 2008, 7, 845-854.
2. L. L. Zhang, R. Zhou and X. S. Zhao, *J. Mater. Chem.*, 2010, **20**, 5983-5992.
3. Y. Zhai, Y. Dou, D. Zhao, P. F. Fulvio, R. T. Mayes and S. Dai, *Adv Mater*, 2011, **23**, 4828-4850.
4. B. E. Conway, New York, 1999.
5. Z. H. Fng, R. S. Xue and X. H. Shao, *Electrochim. Acta*, 2010, **55**, 7334-7340.
6. A. K. Geim and K. S. Novoselov, *Nat. materials*, 2007, **6**, 183-191.
7. A. K. Geim, *Science*, 2009, **324**, 1530-1534.
8. C. N. R. Rao, A. K. Sood, R. Voggu and K. S. Subrahmanyam, *J. Phys. Chem. Lett.*, 2010, **1**, 572-580.
9. D. Chen, L. Tang and J. Li, *Chem. Soc. Rev.*, 2010, **39**, 3157-3180.
10. Y. Zhu, S. Murali, W. Cai, X. Li, J. W. Suk, J. R. Potts and R. S. Ruoff, *Adv Mater*, 2010, **22**, 3906-3924.
11. G. Eda and M. Chhowalla, *Adv Mater*, 2010, **22**, 2392-2415.
12. M. D. Stoller, S. Park, Y. Zhu, J. An and R. S. Ruoff, *Nano lett.*, 2008, **8**, 3498-3502.
13. W. Lv, D. M. Tang, Y. B. He, C. H. You, Z. Q. Shi, X. C. Chen, C. M. Chen, P. X. Hou, C. Liu and Q. H. Yang, *ACS nano*, 2009, **3**, 3730-3736.
14. J. R. Miller, R. A. Outlaw and B. C. Holloway, *Science*, 2010, **329**, 1637-1639.
15. Y. Zhu, M. D. Stoller, W. Cai, A. Velamakanni, R. D. Piner, D. Chen and R. S. Ruoff, *ACS nano*, 2010, **4**, 1227-1233.
16. Y. W. Zhu, S. Murali, M. D. Stoller, A. Velamakanni, R. D. Piner and R. S. Ruoff, *Carbon*, 2010, **48**, 2118-2122.
17. Y. Zhu, S. Murali, M. D. Stoller, K. J. Ganesh, W. Cai, P. J. Ferreira, A. Pirkle, R. M. Wallace, K. A. Cychosz, M. Thommes, D. Su, E. A. Stach and R. S. Ruoff, *Science*, 2011, **332**, 1537-1541.
18. B. G. Choi, M. Yang, W. H. Hong, J. W. Choi and Y. S. Huh, *ACS nano*, 2012, **6**, 4020-4028.
19. P. Yadav, A. Banerjee, S. Unni, J. Jog, S. Kurungot and S. Ogale, *ChemSusChem*, 2012, **5**, 2159-2164.
20. L. L. Zhang, X. Zhao, M. D. Stoller, Y. Zhu, H. Ji, S. Murali, Y. Wu, S. Perales, B. Clevenger and R. S. Ruoff, *Nano Lett.*, 2012, **12**, 1806-1812.
21. T. Kim, G. Jung, S. Yoo, K. S. Suh and R. S. Ruoff, *Acs Nano*, 2013, **7**, 6899-6905.
22. J. H. Lee, N. Park, B. G. Kim, D. S. Jung, K. Im, J. Hur and J. W. Choi, *ACS nano*, 2013, **7**, 9366-9374.
23. L. Wu, H. Feng, M. Liu, K. Zhang and J. Li, *Nanoscale*, 2013, **5**, 10839-10843.
24. L. Zhang, F. Zhang, X. Yang, G. Long, Y. Wu, T. Zhang, K. Leng, Y. Huang, Y. Ma, A. Yu and Y. Chen, *Sci. Rep.*, 2013, **3**, 1408.
25. X.-C. Dong, H. Xu, X.-W. Wang, Y.-X. Huang, M. B. Chan-Park, H. Zhang, L.-H. Wang, W. Huang and P. Chen, *ACS Nano*, 2012, **6**, 3206-3213.
26. Y. Xu, Z. Lin, X. Huang, Y. Liu, Y. Huang and X. Duan, *ACS nano*, 2013, **7**, 4042-4049.

27. J. Zhu, C. Cheng, X. Yang, Y. Wang, L. Qiu and D. Li, *Nat. Chem.*, 2013, **19**, 3082-3089.
28. H. Li, L. Pan, C. Nie, Y. Liu and Z. Sun, *J. Mater. Chem.*, 2012, **22**, 15556.
29. Y. Chen, X. Zhang, H. Zhang, X. Sun, D. Zhang and Y. Ma, *RSC Adv.*, 2012, **2**, 7747.
30. Q. Zhou, J. Gao, C. Li, J. Chen and G. Shi, *J. Mater. Chem. A*, 2013, **1**, 9196.
31. A. Ahmadpour and D. D. Do, *Carbon*, 1996, **34**, 471-49.
32. Q. Jiang, Y. Zhao, X. Y. Lu, X. T. Zhu, G. Q. Yang, L. J. Song, Y. D. Cai, X. M. Ren and L. Qian, *Chem. Phys. Lett.*, 2005, **410**, 307-311.
33. Y. Zhu, S. Murali, M. D. Stoller, K. J. Ganesh, W. Cai, P. J. Ferreira, A. Pirkle, R. M. Wallace, K. A. Cychosz, M. Thommes, D. Su, E. A. Stach and R. S. Ruoff, *Science*, 2011, **332**, 1537-1541.
34. Y. Li, M. van Zijll, S. Chiang and N. Pan, *J. Power Sources*, 2011, **196**, 6003-6006.
35. N. I. Kovtyukhova, P. J. Ollivier, B. R. Martin, T. E. Mallouk, S. A. Chizhik, E. V. Buzaneva and A. D. Gorchinskiy, *Chem. Mater.*, 1999, **11**, 771-778.
36. W. S. Hummers and R. E. Offeman, *J. Am. Chem. Soc.*, 1958, **80**, 1339-1339.
37. C. Gao, X. Y. Yu, R. X. Xu, J. H. Liu and X. J. Huang, *ACS Appl. Mater. Interf.*, 2012, **4**, 4672-4682.
38. X.-h. Meng, X. Shao, H.-y. Li, F.-z. Liu, X.-p. Pu, W.-z. Li and C.-h. Su, *Mater. Res. Bull.*, 2013, **48**, 1453-1457.
39. A. Mathkar, D. Tozier, P. Cox, P. Ong, C. Galande, K. Balakrishnan, A. Leela Mohana Reddy and P. M. Ajayan, *J. Phys. Chem. Lett.*, 2012, **3**, 986-991.
40. Y. Xu, K. Sheng, C. Li and G. Shi, *ACS nano*, 2010, 4, 4324-4330.
41. S. Ye, J. Feng and P. Wu, *ACS Appl. Mater. Interf.*, 2013, 5, 7122-7129.
42. J. Jagiello and M. Thommes, Carbon, 2004, **42**, 1227-1232
43. D. H. Seo, S. Yick, Z. J. Han, J. H. Fang and K. Ostrikov, *ChemSusChem*, 2014, 7, 2317-2324.
44. Y. J. Lee, G.-P. Kim, Y. Bang, J. Yi, J. G. Seo and I. K. Song, *Mater. Res. Bull.*, 2014, **50**, 240-245 and references therein.
45. L. Jiang, J. W. Yan, Y. Zhou, L. X. Hao, R. Xue, L. Jiang and B. L. Yi, *J .Solid State Electrochem.*, 2013, **17**, 2949-2958.